SPEKTRUM INDUSTRI

Journal homepage: http://journal3.uad.ac.id/index.php/spektrum
ISSN 2442-2630 (online) | 1693-6590 (print)

Robust controller numerical design for reinforced concrete structures under seismic excitation conditions

Tim Chena[1], Robert C. Crosbie[2], Azita Anandkumarb[3], Charles Melville[4], J Chen[5]* and T Nguyen[6]

[1] Faculty of Information Technology, Ton Duc Thang University, Ho Chi Minh City, Vietnam
[2] Faculty of Mathematics, Technische Universität Dresden, Dezernat 8, 01062 Dresden, Saxony, Germany 3
[3] Computing and Mathematical Sciences, University of Bath, Bath, BA2 7AY, UK
[4] Department Electrical & Electronic Engineering, University of Bath, Bath, BA2 7AY, U.K.
[5] Department of Artificial Intelligence, University of Maryland, Maryland 20742, USA
[6] Hanoi Cultural University, Hanoi City, Vietnam
*Corresponding Author: cj343965@gmail.com

ARTICLE INFO

Article history
Received: September 2022
Revised : October 2022
Accepted: October 2022

Keywords
genetic design algorithm
Simulation method
Fuzzy logic reasoning : the evolutionary algorithm of bats

ABSTRACT

The article discusses driver optimization design issues that combine the evolution of artificial intelligence of the bat optimization algorithm with fuzzy drivers to enable practical applications in construction. The designation of system controllers includes various subsections such as initial system parameters, EB optimization algorithm, cloud controllers, stability analysis, and excitation sensors. The advantage of this design is the integrated H2 / H∞ output of a robust strategy for certain systems with continuous and polyhedral uncertainties f or. The asymptote was obtained by adjusting the design parameters with the help of correction criteria. Numerical verification of the time and frequency domain shows the new system design to accurately predict and control the structural displacement reactions required to actively control each model structure . The Genetic Algorithm Test technique uses the Hurwitz Matrix Functional Structure hierarchy for hierarchical conditions and measures of exacerbation of effect. This article proposes any type of dynamic controller to obtain the optimal power structure required for active control of nonlinear structures. This method has shown favorable results in the resolutions of closed systems.

INTRODUCTION

A detailed inspection covers the effects and potential hazards of damaging hazards such as earthquakes and construction disturbances. The basic control frame contains a dynamic wet mass that absorbs sudden moisture and prevents gusts of wind from rising to tall structures. Given the important human considerations, experimental research on vibration control structures is expected to be completed as part of the Morning Warning of Earthquakes. Over the past two decades, a great deal of research has been done and applied to the development , generation, testing and implementation of active, semi-active and sub- hybrid regulations. The vibrations are damped by excited unstable structures. The use of external power supplies is an important part of the power dynamism and the dynamics of the linking activity. Multiple inspections have shown that dynamic gadgets have been tested as vibration dampers to reduce structural vibration (e.g. Connor, 2003; Yanıketal ., 2018; Adeli and Jiang)., 2006; Jiang and Adeli, 2005; Muhammad et al. 2018; Zhou et al. 2015 Jin et al. 2018 Li et al. 2017 Chang et al. , 2019). Dynamic mode control is fully applicable to multi-degree structures of freedom as the response is performed in a general manner. External power supplies are inefficient, require no control framework, are increasingly cost effective, and facilitate application planning.

While various ratings and their strategies have been approved and proposed , most of the research concerns the practical applications and methods of fleet regulation. Robust control problems can be divided into linear transform systems and other problems, including time invariant or nonlinear. In general, nonlinear systems can be thought of as nonlinear nonlinear systems. In other words, the problem of nonlinear control can be solved by the robust force method. In other words, reliable design methods can be used to design nonlinear controllers if the nonlinear model can be considered a linear uncertainty model. Based on the concepts and concepts mentioned above, the goal of this article is to design a reliable driver for linear and nonlinear systems, including uncertain model and strong effect. For example, a nonlinear system can be considered a linear system if the state of the system is close to the equilibrium point. According to this concept, the Takagi Kanno concept, whose reasoning (TS) uses the fuzzy concept, is a fuzzy concept combining several linear systems to approximate the behavior of the original non-linear system (Kickert and Mamdani, 1978; Braae and) Rutherford, 1979; Chang and Zadeh. 1972, Buvana and Jayashri, 2019). With this simple and general approach, any model can use a linear system to express the meaning of each power rule. This allows the use of the linear feedback method with continuous feedback. Królów (1996) Proposed distributed power series of parallel concepts (PDC) . It follows the same order as the settings specified in the Hypothesis section for each rule.

An effective theoretical system of building management systems requires a higher level of service standards and an effective way to reduce the initial user experience without harming the building. The literature discusses many reasons to achieve this goal by trying various forms of management, but the correct solution to the problem remains ambiguous. Recently, the Evolutionary Bat Algorithmic (EBA) optimization method has been introduced, which highlights a number of optimization problems. This article is about EBA optimization in construction management strategy, one of the latest interesting optimization optimization topics.

The information gathering zone is also warm and fun, and attracts the attention of many researchers. Lots of people are encouraged and inspired by the algorithm These algorithms are built in the field for the intelligence of natural animals. Methods often require complex calculations and mimic some existing or retained methods. For example, Tsai et al. , (2012) was used to describe the bat discovery process in order to solve many mechanical problems. In this article, the EBA applies to optimizing the building administration plan, which is one of the most difficult optimization problems in recent years. Variable optimization controllers are those that provide response conditions (such as output) to a controller position change.

RESEARCH METHOD

Concrete structures are the most common type of modern architecture. Figure 1 shows that the three-story concrete structure has been reinforced. It usually consists of a specific body or skeleton. The horizontal elements are rays and the vertical elements are columns. Concrete buildings also include floors and roofs that serve as foundations. The poles are so large that they carry the house's luggage.

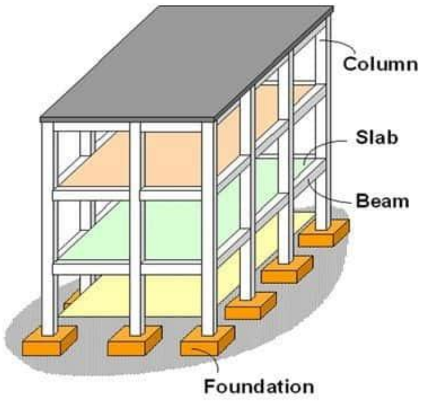

Figure 1. Floor level

equation. (1) The equation of motion of the motor unit and the electronic system of a rock reservoir can be written as a model consisting of the following assumptions (Zhou et al., 2015; Kim et al., 2018; Leeetal., 2018 et al. Chang et al., 2017 Chang et al., 2019: Chen, 2014;

$$M\ddot{\bar{X}}(t)+C\dot{\bar{X}}(t)+K\bar{X}(t)=\bar{B}U(t)-M\bar{r}\ddot{x}_g \tag{1}$$

Where is the vector n representing $\bar{X}=[\bar{x}_1,\bar{x}_2,\cdots\bar{x}_n]^T\in R^n$ the area-to-surface drift from the designated i-th floor of the unit. Matrices M , C, K have mass, and sometimes matrices and matrix matrices respectively . In the controller design, each criterion corresponds to equation (1), and the equation of state is combined with:

$$\dot{X}(t)=AX(t)+BU(t)+E\ddot{x}_g \tag{2}$$

with* $X^T=[\bar{X}^T \quad \dot{\bar{X}}^T]$, $A=\begin{bmatrix}0 & I_{n\times n}\\ -M^{-1}K & -M^{-1}C\end{bmatrix}$ $B=\begin{bmatrix}0\\ M^{-1}\bar{B}\end{bmatrix}$ $E=\begin{bmatrix}0\\ -\bar{r}\end{bmatrix}$.

The dynamic system (2) is different for each region. You can use the fuzzy control TS to build more linear models and link each linear model with an associated function. Figure 2 shows the concept of conceptual inference, which is based on the fuzzy TS pattern.

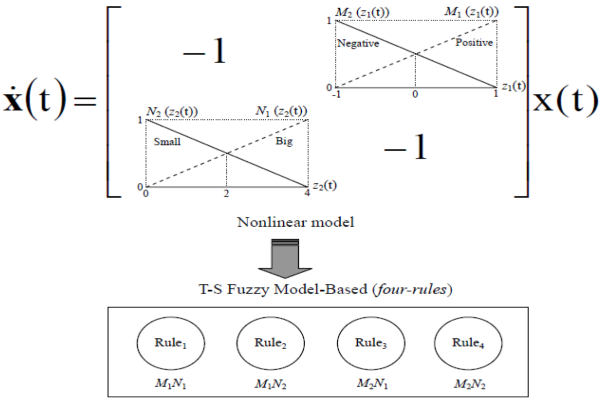

Figure 2. Describe fuzzy models based on TS

Use dynamic models to examine the final time dimension of an independent line installation Σ (θ).

$$\Sigma(\theta):\begin{cases}\dot{\mathbf{x}}(t)=\mathbf{A}(\theta)\mathbf{x}(t)+\mathbf{B}_\omega(\theta)\boldsymbol{\omega}(t)+\mathbf{B}_u(\theta)\mathbf{u}(t)\\ \mathbf{y}(t)=\mathbf{C}_y\mathbf{x}(t)\\ \mathbf{z}_2(t)=\mathbf{C}_2\mathbf{x}(t)+\mathbf{D}_{2u}\mathbf{u}(t)\\ \mathbf{z}_\infty(t)=\mathbf{C}_\infty\mathbf{x}(t)+\mathbf{D}_{\infty\omega}\boldsymbol{\omega}(t)+\mathbf{D}_{\infty u}\mathbf{u}(t)\end{cases}$$

Where x (t) n is the state input, u (t) n is the input , ω (t) n is the disturbance , y (t) n is the measurement output , z2 i Each of the outputs z∞ has appropriate dimensions . The parameters Cy , C2, C∞ derive the matrices y (t), z2 (t) and z∞ (t) , respectively . In addition, the parameters D 2u , D ω ω , D ∞ u are transferred directly from the starting matrices to the outputs y (t), z 2 (t) and z ∞ (t) , respectively . A (θ) B u (θ) Bω (θ) depends on an unknown variable or time variables or a table divided into circles and has the following structure.

$$\mathbf{A}(\theta)=\sum_{k=1}^{r}\theta_k\mathbf{A}_k\ ,\quad \mathbf{B}_u(\theta)=\sum_{k=1}^{r}\theta_k\mathbf{B}_{u,k}\ ,\quad \mathbf{B}_\omega(\theta)=\sum_{k=1}^{r}\theta_k\mathbf{B}_{\omega,k}\ ,\tag{3}$$

where $\{\mathbf{A}_k, \mathbf{B}_{\omega,k}, \mathbf{B}_{u,k}\}$ are constant matrix/vector. This means that the k^{th} edge of Dynamic model; $\theta=[\theta_1,\theta_2,\cdots,\theta_r]\in\Re^r$ is the uncertain vector which belongs to the

$$\Theta=\left\{\theta\in\Re^r:\sum_{k=1}^{r}\theta_k=1,\ \theta_k\geq 0,\ \ k=1,\ 2,\ \cdots,r\right\}.\tag{4}$$

Static output feedback controller

$$u(t)=-\mathbf{G}\mathbf{y}(t).\tag{5}$$

Replacing (5) with (2) closes the loop and restores the system.

$$\Sigma_c(\theta):=\begin{cases}\dot{\mathbf{x}}(t)=\mathbf{A}_c(\theta)\mathbf{x}(t)+\mathbf{B}_\omega(\theta)\boldsymbol{\omega}(t)\\ \mathbf{z}_2(t)=\overline{\mathbf{C}}_2\mathbf{x}(t)\\ \mathbf{z}_\infty(t)=\overline{\mathbf{C}}_\infty\mathbf{x}(t)+\mathbf{D}_{\infty\omega}\boldsymbol{\omega}(t)\end{cases},\tag{6}$$

where $\mathbf{A}_c(\theta)$, $\overline{\mathbf{C}}_2$ and $\overline{\mathbf{C}}_\infty$ are defined in the following mapping:

$$\mathbf{A}_c(\theta)\equiv\sum_{k=1}^{r}\theta_k\left(\mathbf{A}_k-\mathbf{B}_{u,k}\mathbf{G}\mathbf{C}_y\right),\ \ \overline{\mathbf{C}}_2\equiv\left(\mathbf{C}_2-\mathbf{D}_{2u}\mathbf{G}\mathbf{C}_y\right),\text{ and }\ \overline{\mathbf{C}}_\infty\equiv\left(\mathbf{C}_\infty-\mathbf{D}_{\infty u}\mathbf{G}\mathbf{C}_y\right).\tag{7}$$

Our goal is to find an acceptable G that is similar to this;

a) Equation. (6) Sure;

b) the following business monitoring standards:

$$J(\Sigma_c(\theta))=\phi\|H_\infty(s,\theta)\|_\infty^2+\varphi\|H_2(s,\theta)\|_2^2,\tag{8}$$

where $\phi\geq 0$ and $\varphi\geq 0$ are scale factors; i.e,

$$\mathrm{H}_\infty(s,\theta)\equiv z_\infty(s)/\omega(s)\equiv\overline{\mathbf{C}}_\infty(s\mathbf{I}-\mathbf{A}_c(\theta))^{-1}\mathbf{B}_\omega(\theta)+\mathrm{D}_{\infty\omega}\ \text{ and}$$

$$\mathrm{H}_2(s,\theta)\equiv z_2(s)/\omega(s)\equiv\overline{\mathbf{C}}_2(s\mathbf{I}-\mathbf{A}_c(\theta))^{-1}\mathbf{B}_\omega(\theta)\tag{9}$$

H2 and H∞ are the norms of closed loops (6)

$$\|H_2(s,\theta)\|_2=\frac{1}{2\pi}\int_{-\infty}^{\infty}\|\mathrm{H}_2(s,\theta)\|_F^2 ds\ ,\qquad \|H_\infty(s,\theta)\|_\infty\equiv\sup_{s\in\Re}\sigma_{max}(H_\infty(s,\theta)),\tag{10}$$

Where σmax (H∞) represents the maximum value of H∞ and the Frobenii norm.

$$H_2\ \text{ is }\ \|H_2\|_F^2\equiv\left\{\sqrt{\mathrm{trace}(H_2^T H_2)}\right\}.\tag{11}$$

as defined

$$\|H_\infty(s,\theta)\|_\infty^2\ \text{ and }\ \|H_2(s,\theta)\|_\infty^2\tag{12}$$

This can be translated as the maximum value of ω (t) and RMS in any direction and at any frequency, respectively. To achieve this, we obtain the criterion validity of the Lyapunov method as shown in the figure below.

Lemma 1

symmetrical X∞ and G , the ratio is stable over the latitude H∞ or within γ.

$$\begin{bmatrix} \overline{\mathbf{A}}_k^T\mathbf{X}_\infty + \mathbf{X}_\infty\overline{\mathbf{A}}_k & * & * \\ \mathbf{B}_{\omega,k}^T & -\mathbf{I} & * \\ \overline{\mathbf{C}}_\infty\mathbf{X}_\infty & \mathbf{D}_{\infty w} & -\gamma^2\mathbf{I} \end{bmatrix} < 0,\ \text{for}\ \ k = 1,2,\cdots,r, \qquad \overline{\mathbf{A}}_k \equiv \left(\mathbf{A}_k - \mathbf{B}_{u,k}\mathbf{G}\mathbf{C}_y\right) \tag{13}$$

The concept is to describe a term that can be generated from symmetry.

Lemma II

The closed-loop system (2.4) is robustly stable with $\|H_2(s,\theta)\|_2 \le \upsilon$ if there exist a $\mathbf{G}$ and two symmetric matrices $\mathbf{X}_2 > 0$ and $\mathbf{Y} \ge 0$ such that

$$\begin{bmatrix} \overline{\mathbf{A}}_k^T\mathbf{X}_2 + \mathbf{X}_2\overline{\mathbf{A}}_k & * \\ \mathbf{B}_{\omega,k}^T & -\mathbf{I} \end{bmatrix} < 0,\ \text{for}\ \ k = 1,2,\cdots,r \tag{14}$$

$$\begin{bmatrix} \mathbf{Y} & * \\ \mathbf{X}_2\overline{\mathbf{C}}_2^T & \mathbf{X}_2 \end{bmatrix} > 0 \qquad Trace(\mathbf{Y}) \le \upsilon^2 \tag{15}$$

y = 1 , theory predicted by Scherer et al. Easily available since (1997). Therefore, no proof is required. It is obvious (13) that the steady state includes (14). Therefore, the H∞ / H2 mixture can be expressed.

$$\underset{\mathbf{X},\mathbf{Y},\mathbf{G}}{\text{Minimize}}\ \phi\gamma^2 + \varphi\, Trace(\mathbf{Y}) \quad ,\ \mathbf{X} = \mathbf{X}_\infty = \mathbf{X}_2 > 0 \ \text{ and } \ \mathbf{Y} \ge 0 \tag{16}$$

Follow (13) and (15). It is known that the worst case LMI can be used based on the worst case outcome method. Therefore, the dataset can be very conservative. Moreover, by solving LMI by G alone, let X = X2 = X∞> 0 (Scherer et al., 1997). However, these limitations can be minor , especially with robust multi-sided models.

To overcome the above errors, a numerical algorithm is used to find consecutive responses to productions, stabilizing closed loops and asymptomatically obscuring performance circuits. Lapunov's design, general configuration, and experimental techniques used to narrow down the Hurwitz approach to mitigate stability in the family polynomial region (Chung and January 2009) showed solid stability.

Definition 1:

closed dynamical system Ac (θ) can be transformed into a family using a sequential polynomial system with G data

$$\mathcal{P} = \left\{ p(s,\theta) : p(s,\theta) = \sum_{k=1}^{r} \theta_k\, p_k(s);\ p_k(s) = det\left(s\mathbf{I} - \overline{\mathbf{A}}_k\right) \right\} \tag{17}$$

where $\overline{\mathbf{A}}_k \equiv \left(\mathbf{A}_k - \mathbf{B}_{u,k}\mathbf{G}\mathbf{C}_y\right)$, $p_k(s) = a_{n,k}s^n + a_{n-1,k}s^{n-1} + \ldots.. + a_{1,k}s + a_0$, $\forall a_{n,k} = 1$ and $\mathcal{P}$

A polynomial represents a family.

1 Assumption

$$\Gamma_{ij} \equiv \{p_m(s) : p_m(s) = \alpha\, p_i(s) + (1-\alpha)\, p_j(s), \alpha \in [0,1]\}, \tag{18}$$

$$\lambda\left(\mathbf{H}_i^{-1}\mathbf{H}_j\right) \notin (-\infty, 0], \tag{19}$$

where $i, j = 1, 2, \cdots, r$ and $i < j$. $Re_{min}(\bullet)$ and $\lambda(\bullet)$ denote the minimum real part and eigenvalues of $\bullet$, respectively. For is a fixed polynomial $P(s) = a_{n,j}s^n + a_{n-1,j}s^{n-1} + \ldots + a_{0,j}$

nn H_j is the Hurwitz test matrix related to the P (s) table.

Definition 2:

Define the average performance as follows:

$$J(\Sigma_c) := \int_\Theta \left(\phi\|H_\infty(s,\theta)\|_\infty^2 + \varphi\|H_2(s,\theta)\|_2^2\right)d\theta. \tag{20}$$

Moreover, consider only optimizing the vector sum of each uncertainty. How (20) can you say that.

$$J(\Sigma_c) := \frac{1}{r}\left(\sum_{k=1}^{r}\left(\phi\left\|\boldsymbol{H}_\infty(s,\theta_k)\right\|_\infty^2 + \varphi\left\|\boldsymbol{H}_2(s,\theta_k)\right\|_2^2\right)\right) \quad \text{where} \quad \{\theta_1, \theta_2, \cdots, \theta_r\} \in \Theta . \tag{21}$$

Lemma III.

But Σc (θ) is stable in the following cases.

(1) $\mathrm{Re}\left(\lambda_{\max}\left(\overline{\mathbf{A}}_n\right)\right) \le -\psi < 0$, (22).

(2) $\max_{1\le k\le r} \mathrm{Re}\left(\lambda_{\max}\left(\overline{\mathbf{A}}_k\right)\right) \le -\psi < 0$, (23).

(iii) $d_r > 1$, (24).

$$\text{where} \quad \overline{\mathbf{A}}_n \equiv \mathbf{A}_n - \mathbf{B}_n\mathbf{G}\mathbf{C}_y , \quad \mathbf{A}_n \equiv \frac{1}{r}\sum_{k=1}^{r}\mathbf{A}_k \quad \text{and} \quad \mathbf{B}_n \equiv \frac{1}{r}\sum_{k=1}^{r}\mathbf{B}_k . \tag{25}$$

If > 0, the solution is terminated. The stability of the solidity relationship d is defined as follows:

$$d_r \equiv \frac{1+\sum_{i=1}^{r}\sum_{j=i+1}^{r} flag(\Gamma_{ij})}{T_b}, \quad T_b = \frac{r\times(r-1)}{2} \quad flag(\Gamma_{ij}) = \begin{cases} 1 & ; \ Re\left(\lambda_{max}\left(-\mathbf{H}_i^{-1}\mathbf{H}_j\right)\right) < 0 \\ 0 & ; \ \text{else} \end{cases}, \tag{26}$$

According to Lemma 3, the rest of the task is to adjust the optimal G (22-24) and reduce the cost effect (21) . The GA-based floating point designation is shown in Figure G. 3-4 Poll G dominates with good odds (22-24) and (21). To maintain form, we use the hierarchy (22-24) and (21) to bind to a function called HFFS (21). You can search for a G in any GA by changing the HFFS training modes.

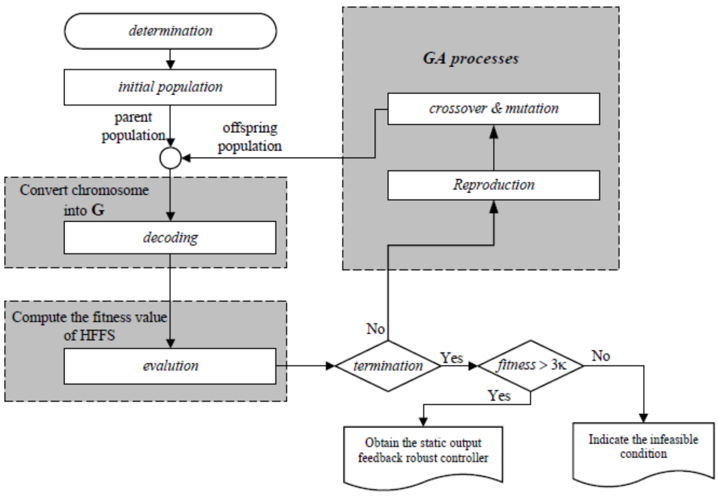

Figure 3. Structural assessment of the developed genetic algorithm

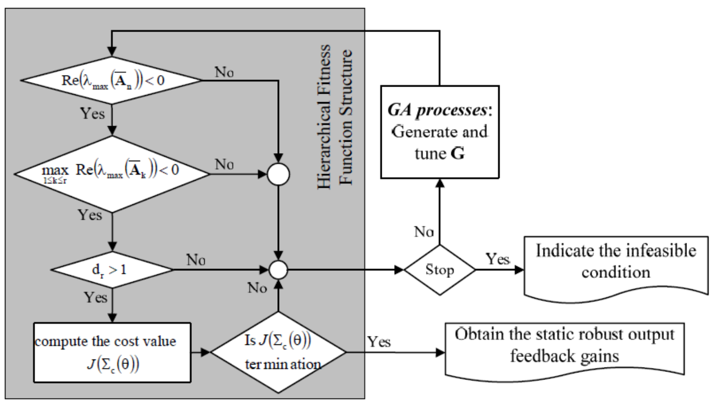

Figure 4. Algorithmic algorithm for estimating genetic structures

The method of performing HFFS is to convert (22-24) into lower body functions and link these lower body functions to a hierarchy. By combining the sequences (22-24) you can turn your subconscious into action.

$$fitness_i \equiv \kappa \times d_i \tag{27}$$

Where efficiency and function are the i-th sub-efficiency. This assessment is based on the ability to more easily identify the stability of the scenery conditions, which are implemented in a coherent hierarchical structure. The execution of di is defined as the corresponding i-th.

$$d_1 \equiv 1 - \psi - Re\left(\lambda_{max}\left(\overline{\mathbf{A}}_n\right)\right), \tag{28}$$

$$d_2 \equiv 1 - \psi - \underset{1 \le k \le r}{max}\ Re\left(\lambda_{max}\left(\overline{\mathbf{A}}_k\right)\right), \tag{29}$$

$$d_3 \equiv d_r\ , \tag{30}$$

$$d_4 \equiv \frac{1}{\underset{1\le k\le r}{min}\ \frac{1}{r}\left(\sum_{k=1}^{r}\left(\phi\left\|\boldsymbol{H}_\infty(s,\theta_k)\right\|_\infty^2 + \varphi\left\|\boldsymbol{H}_2(s,\theta_k)\right\|_2^2\right)\right)}, \tag{31}$$

Where is the relative stability of the left half of the complex plane.

RESULTS AND DISCUSSION

Tellurite glasses TeO_2−TiO_2−ZnO with a composition of (100-x-y)TeO_2-xTiO_2-y ZnO, (x,y)=(15;10) (15;5), (10;15), (10;10), (5;30) and (5;10) mol%, used in this study listed in Table1.

The mass attenuation coefficient μ/ρ of these samples were calculated using the Geant4 toolkit and the WinXCOM application for photon energy ranging from 1 keV to 10 MeV. In Figure.1, the μ/ρ values were presented against photon energy. The μ/ρ values obtained from Geant4 simulations were compared to those calculated by the WinXCOM algorithm, as shown in Figure.2. The values of μ/ρ were used to determine the Z_{eff} values, Figure.3. In Figure.4, the Half-value layer values of the investigated glasses were calculated and plotted. In figure 5 the mean free path values were computed and plotted.

Table 1. list of investigated glasses samples, chemical and atomic composition and density.

		Glasses Samples					
		T85T5Z10	T65T5Z30	T80T10Z10	T75T10Z15	T80T15Z5	T85T15Z10
Compositions (mol%)	TeO_2	85	65	80	75	80	75
	TiO_2	5	5	10	10	15	15
	ZnO	10	30	10	15	5	10
Atomic composition (wt.%)	O	0.206	0.206	0.211	0.212	0.217	0.217
	Ti	0.016	0.018	0.033	0.034	0.050	0.051
	Zn	0.044	0.148	0.046	0.070	0.023	0.047
	Te	0.734	0.628	0.710	0.684	0.710	0.685
Density (g/cm^3)		5.490	5.420	5.420	5.410	5.440	5.400

3.1 Mass attenuation coefficient (μ/ρ)

Figure 5 shows the relationship between the HFFS estimate value and steady state. Of course, if Σc (θ) is constant , training and fitness are always constant, and average performance is generally best.

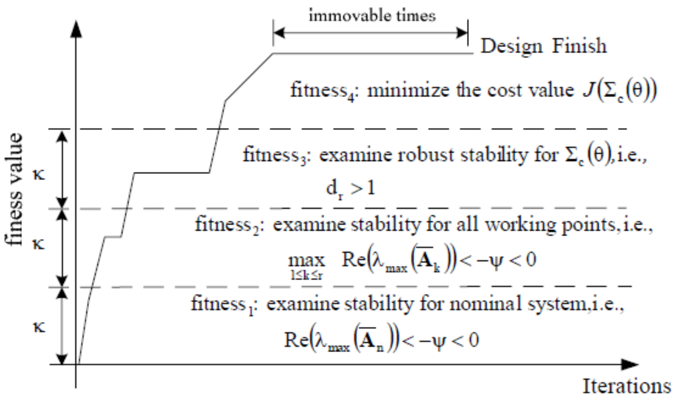

Figure 5. Description of the fit value and number of iterations

The developed algorithm, consisting of the GA defined in HFFS, allows to avoid unusual conditions and select possible states from HFFS.

As a result, physical activity on the computer can be significantly reduced. As shown in Figure 3-4, HFFS is similar to GA. The difference is that an active estimation module can be applied to the HFFS. GA controller code code (BCGA) is shown in the figure. 6.6.

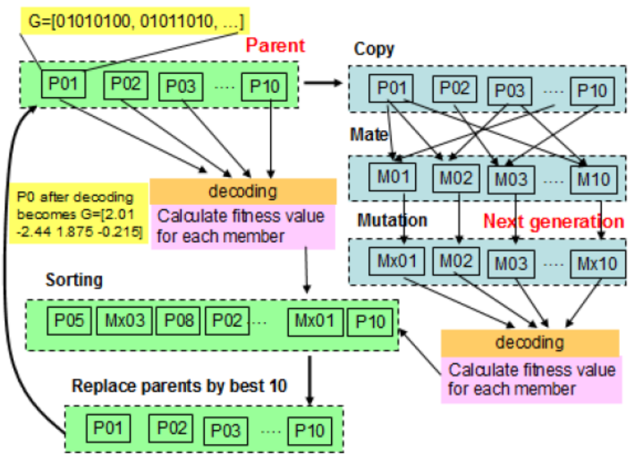

Figure 6. process to find optimal $_{H2}$ / H (output feedback $_{driver}$)

From our previous analyzes it can be concluded that the closure coefficients and the model are closest if the vibrations have a sufficiently high frequency and the appropriate element strength has been selected (Zames and Shneydor, 1976 and. Wang and Abed 1977). , 1995). This allows you to predict the stability of a closed system communicating with the welding system.

4. Stability design and fuzzy EBA algorithm.

From now on, I am not looking for the stability of the original system, but the stability of the system in the cloud. Therefore, the stability criteria are listed below.

Claim.

Any type of system is blocked in a large stable by a PDC if the following LMI conditions are met:

$$QA_i^T(\alpha_m,\beta_m) + A_i(\alpha_m,\beta_m)Q - B_i(\alpha_m,\beta_m)W_i(\alpha_m,\beta_m) - W_i^T(\alpha_m,\beta_m)B_i^T(\alpha_m,\beta_m) < 0 \quad (32).$$

Among them $W_i(\alpha_m,\beta_m) = K_iQ$ _ $W_j(\alpha_m,\beta_m) = K_jQ$

Nick $W_i(\alpha_m,\beta_m)$ Chen $A_j(\alpha_m,\beta_m)$ 2014 $A_i(\alpha_m,\beta_m)$ to be replaced $W_j(\alpha_m,\beta_m)$ No proof needed.

The entire determination process can be summarized as the following algorithm.

How to format the controller described below in a given system?

Selecting the appropriate step size parameter will correctly move the agent into the solution space. This means improving the accuracy of finding the best solutions and reducing the likelihood of local optimization. Medium air was selected in our experiments because bats live in a natural environment of natural air. Here is a brief description of EBA's activities:

Step 1: Randomly assign coordinates to the synthetic material scattered in the solution area.

Step 2: Enter a random number and check if the emission rate is faster than the steady pulse. If the result is positive, we move rashly in the middle of the logarithm of the process.

$$x_i^t = x_i^{t-1} + D \tag{33}$$

where x_i^t i - i - represents the coordinates of the iteration x_i^{t-1} associated with the human agent, represents the coordinates of the agent and itself in the last iteration, and is a unit. D Space represents the journey of two human agents in this iterative system.

$$D = \gamma \cdot \Delta T$$

with* Mean constant corresponding to a γ mathematical mean of his choice . Represents possible experiments and random numbers $\Delta T \in [-1,1]$. For example $\gamma = 0.17$, in the present experiment , air is their medium of choice.

$$[illegible], \beta \in [0,1]$$

with* β Represents a random real number . x_{best} Its coordinates represent the best solution ever found among all human agents. $x_i^{t_R}$ A real person represents new coordinates as a result of a random process of locomotion self-deformation.

Step 3: The Role of the User Defined Exercise builds adaptation and renews it to a suboptimal saved solution.

Step 4: Check the output mode, see if you can go back to step 2 or finish the project and provide a better solution.

The adaptability of the experimental features in evaluation and testing is determined using user-defined criteria. In other words, the educational function is an expression of math in the solution area, and you have to solve the user's problem or find the best solution . Therefore, this article describes a common positive symmetry matrix and educational task on discovering directional forces.

5. Experimental and simulation effects

Consider a building (Yang et al., 1998) in which the structure of each area of the unit is the same. The 76-story building is a vertical ray model. The final model is constructed by treating the structural elements between two adjacent layers as a homogeneous bundle of classical material with a density that assumes 76 degrees of displacement freedom, especially 76 degrees of rotation freedom. Then 76 degrees of freedom are removed with the permanent barrier. It does 76 degrees of freedom . This means that each floor moves to one side. The first five physical frequencies are 0.166, 0.765, 1.992, 3.790, and 6.395 Hz. The RH table for a 76 degree-of-freedom building was calculated using the Rayleigh method and the calculated Moisture Coefficient will be 1% in the first 5 settings. This model has a mass, moisture, and stiffness matrix and is referred to as the "76DOF model". The ATMD equation is constructed

$$\mathbf{M}\ddot{\mathbf{x}} + \mathbf{C}\dot{\mathbf{x}} + \mathbf{K}\mathbf{x} + \mathbf{H}\mathrm{u} = \boldsymbol{\eta}\mathbf{W} \tag{34.}$$

The unit is in the form of a $\mathbf{x} = [\mathrm{x}_1, \mathrm{x}_2, ..., \mathrm{x}_{76}, \mathrm{x}_\mathrm{m}]'$ lock with xi. Matrix of force u control M, C, K, wind excitation W, control effect H and $\boldsymbol{\eta}$ excitation effect.

The resulting equation of state is expressed by the formula:

$$\dot{\mathbf{x}} = \mathbf{A}\mathbf{x} + \mathbf{B}\mathrm{u} + \mathbf{E}\mathbf{W} \tag{35}$$

A unit whose $\mathbf{x} = [\bar{\mathbf{x}}', \dot{\bar{\mathbf{x}}}']'$ total state vector is 48-dimensional. Moreover, in the matrix A represents the ratio , B is (48×1) the action item vector, and (48×48) the unit E is the result of (48×77) the matrix of coefficients excitation .

Likewise, the 76 DOF model (without ATMD building) can be reduced to a 23 DOF system while retaining the original complexity function 46 of the original system. But in these cases, the dimensions A , B , x AE is (46×1) , (46×46) and (46×1) u is respectively (46×76) 0 . The wind load W is naturally generated by an in situ 24DOF (or 23DOF model) wind formed from adjacent settling beams. These simpler examples are represented by W24 with 24 degrees of freedom and W23 with 23 degrees of freedom.

A dimensionless version of the standard performance was designed

$$J_1 = \max\left\{\frac{\sigma_{\ddot{x}1}}{\sigma_{\ddot{x}75o}}, \frac{\sigma_{\ddot{x}30}}{\sigma_{\ddot{x}75o}}, \frac{\sigma_{\ddot{x}50}}{\sigma_{\ddot{x}75o}}, \frac{\sigma_{\ddot{x}55}}{\sigma_{\ddot{x}75o}}, \frac{\sigma_{\ddot{x}60}}{\sigma_{\ddot{x}75o}}, \frac{\sigma_{\ddot{x}65}}{\sigma_{\ddot{x}75o}}, \frac{\sigma_{\ddot{x}70}}{\sigma_{\ddot{x}75o}}, \frac{\sigma_{\ddot{x}75}}{\sigma_{\ddot{x}75o}}\right\} \tag{36}$$

The effective $\sigma_{\ddot{x}i}$ acceleration value of the ith layer is shown here . Unit $\sigma_{\ddot{x}75o}$ = $\mathrm{cm/sec^2}$ 9.824 Indicates excessive acceleration at 75 rms . According to performance and standards J_1, acceleration is limited to 75 floors. This is because the 76th floor is on the top floor of the building and there are no passengers.

The second largest hiring standard is the average free wage above 49 floors.

$$J_2 = \frac{1}{6}\sum_i [(\sigma_{\ddot{x}io} - \sigma_{\ddot{x}i})/\sigma_{\ddot{x}io}] \tag{37}$$

In this case , the acceleration unit is $\sigma_{\ddot{x}io}$ independent of the layers. Metric is the ability to control the restricted area . The standard version is:

$$J_3 = \max\left\{\frac{\sigma_{x1}}{\sigma_{x76o}}, \frac{\sigma_{x30}}{\sigma_{x76o}}, \frac{\sigma_{x50}}{\sigma_{x76o}}, \frac{\sigma_{x55}}{\sigma_{x76o}}, \frac{\sigma_{x60}}{\sigma_{x76o}}, \frac{\sigma_{x65}}{\sigma_{x76o}}, \frac{\sigma_{x70}}{\sigma_{x76o}}, \frac{\sigma_{x75}}{\sigma_{x76o}}, \frac{\sigma_{x76}}{\sigma_{x76o}}\right\} \tag{38}$$

$$J_4 = \frac{1}{7}\sum_i [(\sigma_{xio} - \sigma_{xi})/\sigma_{xio}] \tag{39}$$

The unit is σ_{xi} a unit σ_{xio} with displacement and no control, and unit = 10.112 cm, the layout σ_{x76o} represents the 76th floor of an untamed building.

Each of these objectives must be met in the control so that $\sigma_u \le 100\,\mathrm{kN}$ the capacity constraints are taken into account and $\sigma_{xm} \le 25\,\mathrm{cm}$ where the azimuth outputs and actions are σ_u rms σ_{xm} controlled. In addition to the above limitations, the following factors should be considered and the proposed administrative burden management requirements should be considered.

$$J_5 = \sigma_{xm}/\sigma_{x76o} \tag{40}$$

$$J_6 = \sigma_{\dot{x}m}/\sigma_{\dot{x}76o} \tag{41}$$

This $\sigma_{\dot{x}m}$ speed is run by rms. The performance criteria correspond to the body size (i.e., jump) and potency (i.e., the act of speed) of the agent. For uncontrolled buildings it is $\sigma_{\dot{x}76o}$ 9.28 cm / sec. Where $\sigma_{\dot{x}m}$ is the rms speed of the actuator.

There is a need to perform a statistical simulation (completion) of the proposed application analysis project to estimate its performance based on the following virtual dimensions:

$$J_7 = \max\left\{\frac{\ddot{x}_{p1}}{\ddot{x}_{p75o}}, \frac{\ddot{x}_{p30}}{\ddot{x}_{p75o}}, \frac{\ddot{x}_{p50}}{\ddot{x}_{p75o}}, \frac{\ddot{x}_{p55}}{\ddot{x}_{p75o}}, \frac{\ddot{x}_{p60}}{\ddot{x}_{p75o}}, \frac{\ddot{x}_{p65}}{\ddot{x}_{p75o}}, \frac{\ddot{x}_{p70}}{\ddot{x}_{p75o}}, \frac{\ddot{x}_{p75}}{\ddot{x}_{p75o}}\right\} \tag{42}$$

$$J_8 = \frac{1}{6}\sum_i [(\ddot{x}_{pio} - \ddot{x}_{pi})/\ddot{x}_{pio}] \quad \text{Ad i = 50, 55, 60, 65, 70 and 75} \tag{43}$$

$$J_9 = \max\left\{\frac{x_{p1}}{x_{p76o}}, \frac{x_{p30}}{x_{p76o}}, \frac{x_{p50}}{x_{p76o}}, \frac{x_{p55}}{x_{p76o}}, \frac{x_{p60}}{x_{p76o}}, \frac{x_{p65}}{x_{p76o}}, \frac{x_{p70}}{x_{p76o}}, \frac{x_{p75}}{x_{p76o}}, \frac{x_{p76}}{x_{p76o}}\right\} \tag{44}$$

$$J_{10} = \frac{1}{7}\sum_i [(x_{pio} - x_{pi})/x_{pio}] \quad \text{For i = 50, 55, 60, 65, 70, 75 and 76} \tag{45}$$

Here , peak x_{pi} displacement $\ddot{x}_{pi}$, peak acceleration, and uncontrolled x_{pio} peak displacement all have corresponding acceleration measurements. For example x_{p76o} = $\ddot{x}_{pio}$ 26 009 cm i $\ddot{x}_{p75o}$ = 26 334 cm / 2 sec.

The analysis of the limiting motion of the compression response is as follows : The maximum possible force $\max|u(t)| \leq 300\,\text{kN}$ factor and the maximum possible stroke is $\max|x_m(t)| \leq$ 75 cm. Proof of sem

$$J_{11} = x_{pm}/x_{p76o} \text{ and } J_{12} = \dot{x}_{pm}/\dot{x}_{p76o} \tag{46}$$

where x_{pm}, $\dot{x}_{pm}$ peak actuator stroke speed and peak $\dot{x}_{p76o}$ speed = 22.422 cm / s in 76 layers without power.

However, this limitation does not apply to administrative profits as the overall government influence over the overall system is relatively small. Table 1 shows that all EBA test variables were used. In accordance with the above-mentioned by genetic learning, the number of individuals is 9, the number of individuals is eleven, the migration rate is 0.72, the mutation rate is 0.12, the maximum number of generations is 13. Now $\hat{\theta}$ select the initial GA vector parameter value as follows :

$$[1,\ 0.61, 0.31, 0.11, 0.085, 0, -0.085, -0.11, -0.31, -0.52,\ -1]^T$$

Table 2. EBA parameters above

Boundary condition between positive fixed matrix and regulator gain	-5, 5.
with very little material	air
Run with numbers	4 0
__ population size	2 6
Repeat the entered number	700 700

Like other computational algorithms and evolutionary methods, these EBAs definitely need iteration to find the next solution. Therefore, the same number probability test must be repeated several times over a long period of time to check that the convergence of the results is constant and constant. The number of methods listed in Table 1 and figure 7 are intended to provide some numerical experimental results for testing with statistical methods. In this article, we select a specific number of iterations for the excellence condition. The multimedia material is selected for use in the transmission of waves in the air because it is adapted to the natural environment in which the club is located.

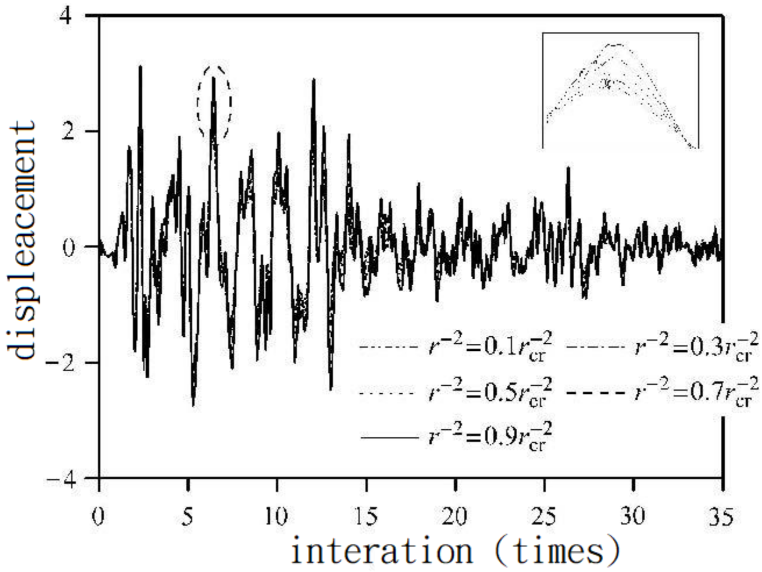

Figure 7. Displacement stability

CONCLUSION

Therefore , the theory of control has influenced many researchers in recent years. Many numerical methods are still proposed in the literature to achieve this great goal by experiencing different forms of government, but they all have some difficulties in getting the right problem. The EBA algorithm is one of the leading innovative optimization methods that can provide researchers with solutions for various optimization. The EBA uses this white paper to optimize the administrative meetings in the building. The optimization parameter is the controller input and the response state provides the output to change its position relative to the engine curve. In this example, there are also new standards for ensuring system stability. This simple and systematic approach to point control helps to deal with external stimuli affecting complex mechanical systems.

REFERENCES

Adley H, Jiang XM (2006) Dynamic model of neural network with fuzzy wavelets for identification of structural systems. International Journal of Structural Engineering (ASCE): *132*(1): 102-111.

Afshar, A. et al. Assessment of the corrosion resistance of basic materials with the use of various types of concrete with various modified coatings and additives. Construction and Construction of Materials, 2020 262: 120034.

Al-Amoudi, OSB, et al. The durability of Continental pozzolani Saudi Arabia concrete is natural as an auxiliary support material. Progress in Concrete Construction, 2019.8 (2):

Alaskar, A. et al. Thermal resistance of concrete columns under axial load. Progress in concrete construction by 2020. 9 (4): 355-365.

Experimental studies of the mechanical properties of Ali Toghroli, PM, Ali Shariati, Reza Bani Ardalana, Mahdi Shariati, Saeed Mafipoor and various reinforced concrete alloys. Concrete construction progress, 2019.

Bedirhanoglu, I. (2014), "Practical model of neuro-fuzzy evaluation of the modulus of concrete elasticity", Structure. United Kingdom Mechanics, 51 (2), 249-265. https://doi.org/10.12989/sem.2014.51.2.249

Benyahia, A. and M. Ghrici, Natural volcanic behavior of gray primed mortar in hot, self-healing climates. Progress in concrete construction, 2018.6 (3).

Chen, T., Khurram, S. and Cheng, C. (2019), "Relief from structural mechanical control and fuzzy control for dynamic analysis of interaction with the structure of fluids," English. Computer, *36*(7), 2200-2219

Chen, T., Khurram, S. and Cheng, C. (2019), "Relief from structural mechanical control and fuzzy control for dynamic analysis of interaction with the structure of fluids," English. Computer, *36*(7), 2200-2219

Chung H. and Chan S., Based on GA H2, H∞ Designing Static Feedback Using Medium Efficiency Concepts and Techniques, "Applications of an Expert System," (43).

Connora JJ. Structural motion control overview. Prentice Hall: Saddle River, New Jersey, 2003

Eswaran, M. and GR Reddy, Numerical Simulation of Tank Design Systems Customized with a Sigma Solution Based on Fluid Transformation and Structuring, Wind Struct, 23 (5), 421-447, 2016.

Farzampour, A., Effect of heat and humidity on mortar injection behavior. Progress in concrete construction, 2017.5 (6): 659-669.

Hosseinpour, E. et al. Concrete pipe, hollow pipe and steel structure direct shear behavior with a thin outer layer of diamond beams. Steel and Composite Structures, 2018. XXVI (4): 485-499.

Kalman, R.E. (1963). New additions to the theory of Wiener Colum In JL Bogdanov and F. Kozin (eds.), Protocols from the 1st Symposium on the theory of random functions and engineering applications of probability. Antwerp John Wiley & Sons

Li, D. et al. Softener for polymers, silica fumes and crushed bullet holes in factory concrete. Intelligent Structures and Systems, 2019. XXIII (2): 207-214.

Lou , L. T., Chen, W. L. and Tang, J. P., (1998) LQG / LTR regulation mode of active control structures, *J. Lat. Mecha.* , ASCE 124 (4) : 446-454

Luo L. et al. Explanation of concrete structures with seismic separation during long short-circuit earthquakes. Development of concrete construction, 2010 9 (1): pp. 71-82.

Mossaheb S., (1983) "Application of mean techniques to study jitter in nonlinear systems", Int. J. de Imperio, 38, 557-576.

Muhammed Arif Sen, Mustafa Tinkir, Mete Kalyoncu, (2018) "Optimization of the PID controller for two-story seismic-driven structures in a bee-grounded algorithm", Journal of Local Frequency Sound Vibration and Active Control 37 (1): 146134841875790

Naghipour, M. et al. The effect of gradual iron shear on the behavior of a concrete foundation strengthens the building. Steel and Composite Structures, 2020. 35 (2): pp. 279-294.

Paknahad, M. et al. , the shear strength equation for channel shear connections in composite steel-concrete beams. Steel and Composite Structures, 2018. XXVIII (4): pp. 483-494 .

Preumont, A. Active Control of Vibratory Structures: An Introduction, Springer (2010)

Razavi, A., PP Sarkar, Laboratory study of translational effects on tornado flow fields near the Earth, Wind structure, 26 (3).

Safa, M., Shariati, M., Ibrahim, Z., Toghroli, A., Baharom, SB, Nor, NM and Petkovic, D. (2016), "Adaptation to the evaluation of factors influencing a validated concrete system for resistance to shear. Neurophagia Composite wood ", composite steel. Structure, interpretation. J., 21 (3), 679-688. Scs.2016.21.3.679

Shariat, M., Shariat, M., Madadi, A. and Wakil, K. (2018), "Optimization of the Lagrange Multiplier Method in Multiplicative Mode and Sensitivity Analysis. Interest in Stabilized Rectangular Concrete Beams", SteelCompos. Structure, interpretation. J., XXIX (2), 243-256 http://dx.doi.org/10.12989/scs.2018.29.2.243

Shariati, M. et al. New Extreme Gray Wolf Optimizer (ELM-GWO) hybrid machine learning model for predicting the compressive force of concrete that partially replaces cement. Computer Engineering, 2020: pp. 1-23.

Shariati, M. et al. Experimental study of the effect of cement materials on the basis of the mechanical properties of a new self-fulfilling concrete. Progress in Concrete Construction, 2019.8 (3).

Shariatmadar, H. and Razavi, HM (2014), "Reaction of Seismic Inspection of Structures Using ATMD with Fuzzy Logic Controller and PSO Method", Structures. United Kingdom Mechanika, 51 (4), 547-564 https://doi.org/10.12989/sem.2014.51.4.547

Sharma, SK, G. Ransinchung, and P. Kumar, Study of SCC Fabrication Using Wollastonite Microfibers. Progress in concrete construction, 2018.6 (2).

Son, L., Bur, M., Rusli, M., Adrianan, A. (2016), "Double dynamic damper design to reduce the vibration system by two degrees of freedom", Structure. United Kingdom Mechanics, 57 (1), 161-178. https://doi.org/10.12989/sem.2016.57.1.161

Stein, G., and Asans, e.g. , (1987). "LQG / LTR multi-variable feedback control design procedures", IEEE. Events from vol. AC-32 2.

Steinberg AM and I. Kadushin (1973) "Stabilization of nonlinear jitter control systems", J. Math. Analysis and Applications 43, 273-284.

Toghroli, A. et al. Assess the use of recycled aggregate concrete and added pozzolanic fibers by using dispersed and recycled industrial fibers. Construction and Construction of Materials, 2020 252: 118 997.

Kai, P. Bread W., j. S., Liao, B. Y., Cai, M. J. and I. Standa, V. , (2012). Algorithms from bat algorithms inspired to solve numerical optimization problems, *Applied Mechanics and Materials* , 148, 134-137 .

Tsai, PW, Hayat, T., Ahmad, B. and Chen, CW (2015), "Simulation and control of structural systems based on the NN-based fuzzy model", Struct. United Kingdom Mechanics, 56 (3), 385-407 https://doi.org/10.12989/sem.2015.56.3.385

Wang, HO and K. Tanaka, (1996) "LMI-Based Fuzzy Stable Non-Line Control Systems and its Applications in Chaos Control", IEEE Int. Meeting. Near the abandoned system, 1433-1438.

Wang HO, K. Tanaka, and MF Griffin, (1996) "Fuzzy control methods for nonlinear systems: stability and design issues", IEEE Trans. Archaeological System 4, 14-23.

XIe, Q., et al. The experimental effect of CFRP on the concrete-beam column was confirmed. Steel and Composite Structures, 2019. 30 (5): 433-441.

Xu, C. et al. Basic design of concrete structures using the genetic algorithm approach. Artificial and Mechanical Engineering, 2019 71 (5).

Yang, JN, JC Wu, AK Agrawal, Z. Li, "Shift Mode Control for Nonlinear and Hysteretic Structures", *J. Lat. Moss* . 12, pp 1330-1339, 1995

Yang, JN, Wu, JC, Samali, B. and Agrawal, AK (1998), "Prove Benchmark Problem for Response Control of Wind-Induced High Buildings", Proc. World Conference on Structural Control, vol. 2, 1407-1416 , John Wiley & Sons, New York.

Yu, L., S. Zhou, and W. Deng, Properties and reaction levels of pozzolan tuff in cement-earthed composites. Development of concrete construction, 2015. 3 (1): 71-90.

Y. Zandi, M. Shariati, A. Marto, X. Wei, Z. Karaca, D. Dao, A. Toghroli, MH Hashemi, Y. Sedghi, Wakil, K. Khorami. M. (2018), "Computer study of comparative analysis of earthquake-affected cylinder stores", SteelCompos. Structure, interpretation. J., XXVIII (4), 439-447 http://dx.doi.org/10.12989/scs.2018.28.4.439

Zhang, Y. (2015), "A method of predicting latigue life based on a fuzzy residual force", Struct. United Kingdom Mechanics, 56 (2), 201-221. https://doi.org/10.12989/sem.2015.56.2.201

Zhou, X., Lin, Y., and Gu, M. (2015), "Multiplex Mass Attenuation Optimization for Long Span Roof Structures under Wind Load", Wind Struct. 20 (3), 363-388. https://doi.org/10.12989/was.2015.20.3.363

Ziaei-Nia, A., M. Shariati, and E. Salehabadi, Dynamic Optimization of High Performance Concrete Mixing Design. Steel and Composite Constructions, 2018. XXIX (1): 67-75.